Precipitation Hardening in 350 Grade Maraging Steel

U.K. VISWANATHAN, G.K. DEY, and M.K. ASUNDI

Evolution of microstructure in a 350 grade commercial maraging steel has been examined. In the earlier stages of aging, the strengthening phases are formed by the heterogeneous precipitation, and these phases have been identified as intermetallic compounds of the Ni_3 (Ti, Mo) and Fe_2Mo types. The kinetics of precipitation are studied in terms of the activation energy by carrying out isothermal hardness measurements of aged material. The mechanical properties in the peak-aged and overaged conditions were evaluated and the flow behavior examined. The overaging behavior of the steel has been studied and the formation of austenite of different morphologies identified. The crystallography of the austenite has been examined in detail. From the microstructural examination of peak-aged and deformed samples, it could be inferred that the dislocation-precipitate interaction is by precipitate shearing. Increased work hardening of the material in the overaged condition was suggestive of looping of precipitates by dislocations.

I. INTRODUCTION

A number of studies have been carried out in the past on the microstructural aspects of different grades of maraging steels.[1,2] A majority of these studies had been in the late sixties and the early seventies. After the lapse of nearly a decade, interest in this type of steels has recently been revived, as reflected in the series of publications on different maraging alloys of Fe-Ni-Co-Mo and Fe-Ni-Mn types.[3,4,5] The manganese-free maraging steel, which is the subject of study in this work, is different from other manganese-free maraging steels of the types T-250 and C-250 on which a considerable amount of work has been done recently.[6,7] The important difference between the steel used in this work and the T-250 and C-250 grade steels can be noticed from Table I, in which the chemical compositions of these steels are given. T-250 is cobalt free, and C-250 contains relatively little titanium. The steel used in the present investigation, on the other hand, contains both cobalt and titanium in a substantial amount. A high-titanium concentration leads to a larger volume fraction of the Ni_3Ti type of phase, and the presence of cobalt makes the formation of the Fe_2Mo type of phase easier.[7] The initial strength of these steels is achieved by the precipitation of a Ni_3 (Ti, Mo) type of phase.[7] This is then followed by precipitation of the Fe_2Mo phase which is responsible for the peak strength and also for maintaining high strength on prolonged aging.[3] With this steel being a precipitation-hardenable alloy, the dislocation-precipitate interaction assumes considerable significance. Though this aspect has been discussed by some workers,[7] experimental studies to examine it are rather few in other category of maraging steels and nonexistent in the category of steel used in the present study. One of the objectives of this work is to ascertain the nature of the dislocation-precipitate interaction at different stages of hardening. This task is made difficult by the fact that the volume fraction of precipitates is not very small, and these precipitates are associated with large strain fields. Other objectives of the microstructural studies are the following: identifying the precipitate phases responsible for strengthening, examining the morphology of precipitates, delineating the sequence of precipitation, and investigating austenite reversion.

U.K. VISWANATHAN, Scientific Officer, Radiometallurgy Division, and G.K. DEY, Scientific Officer, Metallurgy Division, are with Bhabha Atomic Research Centre, Bombay-400085, India. M.K. ASUNDI, 44, Vibha, Government Colony, Bombay-400051, India, is a Private Metallurgical Consultant.

Manuscript submitted August 7, 1992.

II. EXPERIMENTAL

The material used was vacuum arc-melted and vacuum arc-remelted quality 350 grade commercial maraging steel produced by Mishra Dhatu Nigam Limited. The material was in the form of forged and machined bars of 70-mm diameter in double solution annealed condition, a process which consisted of heating the material at 950 °C for 2 hours followed by air cooling and a second annealing at 820 °C for 3.5 hours. The chemical composition of the alloy is given in Table I.

The cylindrical samples used for dilatometry were 12.5 mm in diameter and 10 mm in length machined out from the raw stock with the length of the sample being along the long axis of the bar. A quartz tube dilatometer with manual heating and cooling capabilities was employed. The change in length of the sample was measured using a calibrated dial gage with an accuracy of ±0.0005 mm. The samples were heated to 825 °C at a heating rate of 4 °C/min, held at that temperature for 1 hour, and then cooled to room temperature. The cooling rates achieved during the experiments were 20 °C/min, up to 400 °C/min and 8 °C/min thereafter to room temperature.

Hardness measurements, on a Rockwell C scale, were taken on metallographically polished specimens. Volume fraction of austenite was estimated from the same samples prepared for metallography. A graphite monochromated-Cu K_α radiation was used. The minimum sample area used was about 10 × 10 mm. The $(110)_M$ and $(111)_A$ peaks were selected for analyzing the martensite and the austenite phases respectively.

Thin foils for transmission electron microscopy (TEM) were prepared by window technique and by jet thinning (for deformed samples) using an electrolyte containing

Table I. Chemical Composition of Maraging Steels (in Weight Percent)

Element	Type of Maraging Steel		
	Used in This Work	C-250[7]	T-250[7]
C	0.005	0.015	0.013
Ni	18.39	18.36	18.36
Mo	3.99	4.75	3.02
Co	12.32	8.18	0.11
Ti	1.63	0.46	1.34
Al	0.12	0.12	0.11
Fe	balance	balance	balance

60 pct methanol, 34 pct n-butanol and 6 pct perchloric acid. The temperature of the electrolyte was kept below −30 °C. Microstructural examinations were carried out in a JEOL 2000 FX electron microscope.

III. RESULTS

A. *Dilatometric Studies*

Figure 1 shows typical dilatometric heating and cooling curves obtained from a specimen in an as-solution-treated condition. The change in length of the specimen was plotted against temperature as percentage change. Different characteristic temperatures obtained during the experiment are marked on the curve. During heating, the curve could be considered to be approximately linear close to 500 °C. The point at which the curve deviated from linearity is identified as P_s, the precipitation start temperature. Just above this temperature, a marginal depression could be noticed. Beyond 650 °C, which has been designated as the A_s (the austenite reversion start) temperature, a large contraction could be noticed up to 750 °C, which is the A_f (the austenite reversion finish) temperature. Thereafter, the curve moves up linearly as the temperature of the specimen is raised up to 825 °C.

The cooling curve of the specimen is shown below the heating curve. The curve could be considered linear up to 225 °C, which is the M_s (the martensite transformation start) temperature. A well-defined increase in dilation could be noticed as the temperature of the specimen is reduced further. At around 100 °C, the M_f (the martensite transformation finish) temperature, the curve levels off. From M_f to room temperature, the curve is linear, with only a marginal expansion.

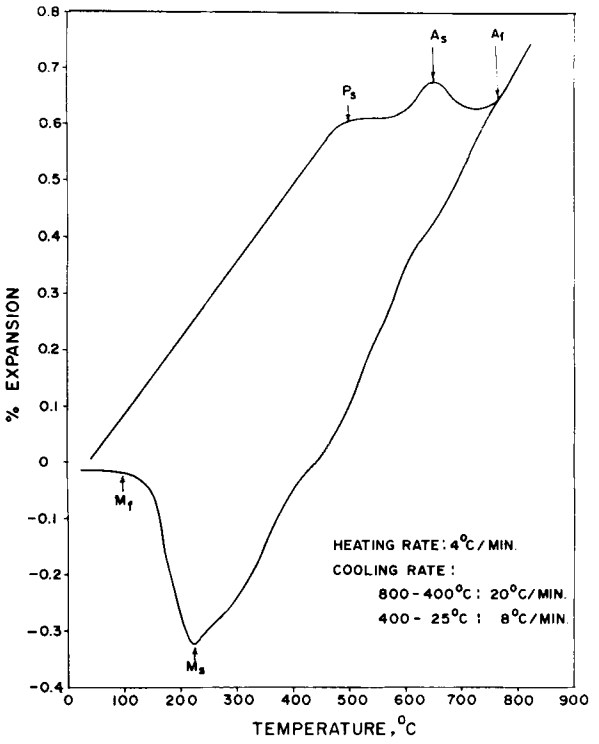

Fig. 1—Dilatometric heating and cooling curves.

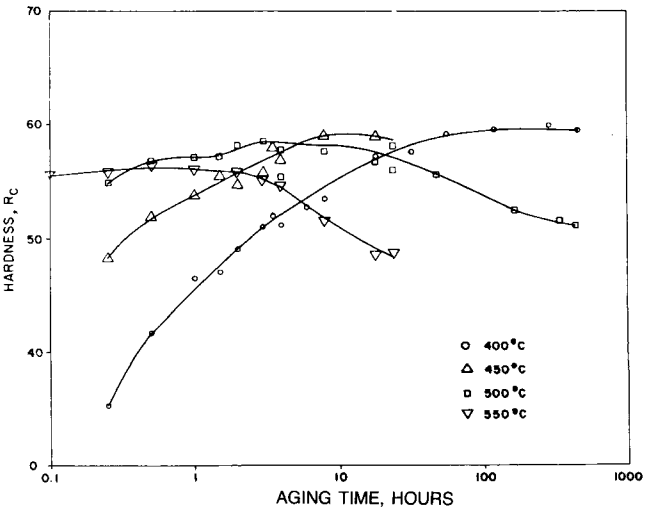

Fig. 2—Hardening response of the material subjected to isothermal aging at different temperatures.

B. *Effects of Aging on Mechanical Properties*

1. *Hardening response*

Figure 2 shows the hardening response of the material exposed to different temperatures and time periods. The hardness of the as-solution treated material was 32 RC. It could be noticed from Figure 2 that the aging response is so fast that there is no indication of an incubation period for the onset of precipitation. The material showed typical precipitation-hardening characteristics in which the maximum hardness was attained on progressively shorter aging as the aging temperature was raised. At 400 °C, a plateau in the hardness curve was observed after 56 hours of aging, and no softening of the material could be noticed even after 500 hours. At 450 °C, no discernible softening could be noticed after aging for 24 hours. At 500 °C, the material attained its peak hardness within 3 hours, whereas at 550 °C, the maximum hardness was attained in 30 minutes. In the text that follows, the material heat treated to the hardness levels on the ascending portion of the hardness time plot is referred to as "underaged" and to the hardness levels on the descending portion as "overaged." It can be seen from Figure 2 that at an aging temperature of 550 °C, the steel exhibited excellent resistance against overaging for nearly

3 hours. Hardness of 48RC was retained even after about 20 hours of aging at this temperature.

The results from the isothermal hardness experiments were used for estimating the activation energy for the precipitation reaction. The time (t) taken to attain peak hardness at each aging temperature (T) was used for estimating the activation energy for the precipitation reaction. By plotting the logarithm of the time taken to attain the peak hardness against $1000/T$, the results could be fitted into an Arrhenius type of equation,

$$\ln(t) = Q/RT + \text{constant} \quad [1]$$

where Q is the activation energy for the precipitation process, R, the universal gas constant, and T, the temperature of aging in Kelvin. The result is presented in Figure 3. Least square regression was used to fit a straight line to the data points and an excellent fit was obtained. An activation energy of 164 ± 4 kJ/mol was obtained from the slope of the straight line.

2. *Mechanical properties of as-solution treated, peak-aged, and overaged material*

Room-temperature mechanical properties of the steel in as-solution-treated, peak-aged, and overaged conditions are given in Table II. The volume fraction of austenite present in the material after each heat treatment is also included in Table II. It can be seen that the material after aging at 510 °C for 3 hours showed remarkable increase in yield and tensile strength accompanied by a considerable decrease in uniform and total elongation. The load elongation data were analyzed in terms of the Ludwik[8] equation

$$\sigma_t = \sigma_0 + K(\varepsilon_p)^n \quad [2]$$

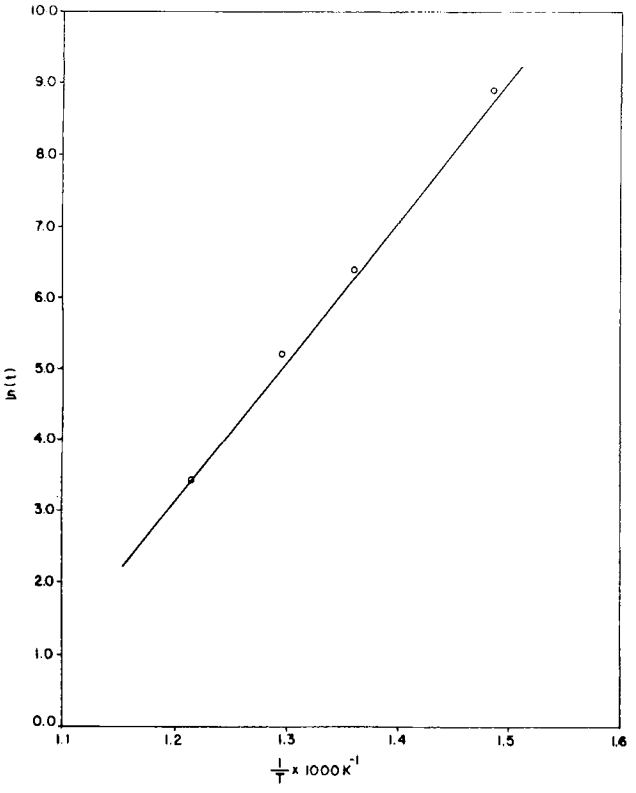

Fig. 3—Arrhenius plot from hardness data for estimating the activation energy for precipitation.

where σ_t is the true stress, σ_0 is the stress corresponding to the point of intersection of the elastic and plastic regimes in the stress-strain curve, K is the material constant, and ε_p is the true plastic strain. It is clear from Table II that the work-hardening exponent of the alloy has substantially reduced after aging. The room-temperature impact toughness was reduced from 190 J for the unaged material to 12 J after aging for 3 hours at 510 °C.

With continued overaging, the tensile strength of the material was substantially reduced and the tensile ductility considerably improved. The work-hardening exponent showed progressive increase with overaging. From Table II, it can also be noticed that prolonged overaging led to the loss of impact energy achieved during the initial stages of overaging.

C. *Microstructural Studies*

1. *Undeformed microstructure*

a. *Microstructure of as-solution-treated, underaged, and peak-aged material*

The microstructure of the sample quenched from the austenitizing temperature consisted of lath martensite. The substructure of the martensite phase was made up of a high density of dislocations. No evidence of microtwins within the laths could be seen in the regions examined. Figure 4 shows a selected area diffraction (SAD) pattern from the as-quenched microstructure. No evidence of precipitation during quenching, either in the form of streaks or of stray spots, could be seen. Though the determination of a habit plane was difficult due to the lack of retained austenite, the martensite-lath boundary plane was found to be close to $\{011\}_M$. The $\langle 111\rangle_M$ directions associated with this plane were found to be parallel to the long axes of the laths.

Specimens aged at 510 °C for 30 minutes were examined to study the early stages of precipitation. Figure 5(a) shows the microstructure of such a specimen. The lath morphology was very similar to that seen in the as-solution treated specimen. Prior austenite grain boundaries could be seen in certain regions. Mostly one particular martensite variant was found to be dominant in each packet. The SAD patterns from the matrix showed precipitate spots and streaks (Figure 5(b)). In the $\langle 111\rangle$ patterns, the streaks appeared to be along the $\langle 110\rangle$ direction. Dark-field microscopy using reflections from the precipitate indicated that the precipitates had fine needle-shaped morphology (Figure 5(c)). The precipitates were found to be aligned along two directions.

Thin foils of specimens aged at 510 °C for 3 hours showed predominantly the presence of a martensite phase. In the SAD patterns taken from the martensite matrix, very strong streaks could be seen. In addition to the streaks, clear diffraction spots, other than those arising from the matrix, could also be seen (Figure 6(a)). Dark-field microscopy, carried out by using these additional diffraction spots, indicated that these originated from the rod-shaped precipitate phase (Figure 6(b)). The precipitate size, on the average, was found to be about 40 nm in length and about 2.5 nm in thickness. The precipitates, though quite small, were found to show a variety

Table II. Room-Temperature Mechanical Properties of the 350 Grade Maraging Steel in As-Solution Treated, Peak-Aged, and Overaged Conditions

Heat Treatment	UTS (MPa)	0.2 Pct YS (MPa)	Elongation (Pct)		Work-Hardening Exponent, n	Impact Energy (J)	Austenite (Pct)
			Total	Uniform			
As-solution-treated	1084	935	13.1	1.5	0.20	190	Nil
Peak-aged at 510 °C for 3 h	2227	2195	5.3	0.8	0.05	12	Nil
Overaged at:							
640 °C for 1 h	1715	1504	10.7	4.1	0.25	20	8
640 °C for 2 h	1615	1414	11.3	5.3	0.30	49	13
640 °C for 4 h	1534	1308	12.2	6.4	0.37	21	22
640 °C for 6 h	1474	1211	12.2	7.3	0.40	20	23
640 °C for 8 h	1458	1203	13.1	6.5	0.42	12	24

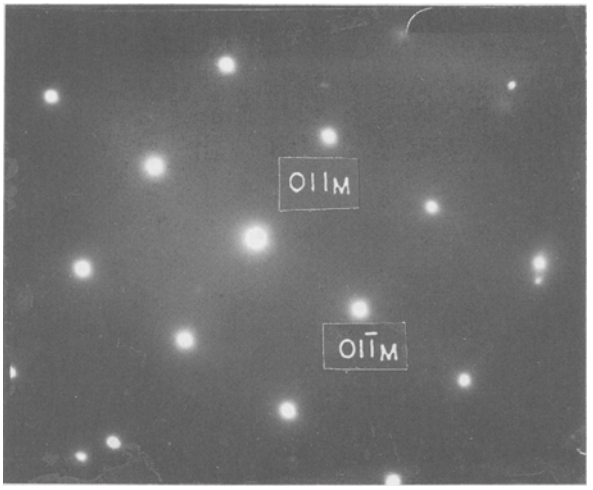

Fig. 4—$[100]_M$ SAD pattern from the martensite phase in the as-quenched microstructure.

of fringe contrast which could be seen clearly in the dark-field images obtained by using precipitate reflections. For certain electron beam directions, these fringes were found to be parallel to the length of the precipitates (Figure 6(c)). In some precipitates, however, the fringes were found to be perpendicular to their length.

The SAD patterns from the precipitates in the specimens aged for 30 minutes and 3 hours at 510 °C (Figures 5(b) and 6(a)) could be indexed in terms of the hexagonal, Ni_3Ti type, eta (η) phase having lattice parameters a = 0.5101 nm and c = 0.8307 nm. Since this phase has been found to contain Mo also,[7] in the text that follows, it will be designated as Ni_3 (Ti, Mo) phase.

In addition to the rod-shaped precipitates, the specimens aged at 510 °C for 3 hours showed the presence of nearly spherical precipitates, as shown in Figure 7(a). Selected area diffraction patterns from these particles could be indexed in terms of the hexagonal Fe_2Mo phase having a = 0.4745 nm and c = 0.7754 nm (Figure 7(b)).

b. *Microstructure of overaged material*

For characterizing the microstructure of the overaged steel, two extreme aging temperatures, namely, 575 °C and 640 °C, were selected.

c. *Specimen overaged at 575 °C for 8 hours*

Thin foils of specimens subjected to this heat treatment showed martensite as the predominant phase. The martensite substructure in these specimens was not much different from that obtained from the specimens aged at 510 °C for 3 hours. However, the former contained a substantial quantity of austenite while the latter was free of austenite. This phase was present mostly between the martensite laths and could be placed in the category of inter-lath austenite (Figure 8(a)). The SAD pattern (Figure 8(b)), taken from the regions containing martensite and austenite phases and the corresponding key (Figure 8(c)), showed that the two lattices obeyed the Nishiyama Wassermann (N-W)[9,10] orientation relationship, which can be stated as $(110)_{bcc}$ // $(111)_{fcc}$ and $[100]_{bcc}$ // $[110]_{fcc}$.

In addition to the lath austenite, recrystallized austenite could also be observed as shown by the arrow in Figure 8(d). This morphological form of the austenite was also found to obey the N-W orientation relationship.

As in the case of the specimens aged at 510 °C for 3 hours, specimens aged at 575 °C for 8 hours also showed a homogeneous distribution of second phase particles of the Ni_3 (Ti, Mo) type phase. Streaks continued to be seen in the diffraction patterns from the precipitates (Figure 8(b)). The average precipitate size was found to be nearly 80 nm in length and 6 nm in width.

The precipitates were found to exhibit two types of fringe contrast:

(1) fringes mostly parallel to the length of the precipitates (Figure 8(e)) due to the size and orientation of the precipitates; and
(2) fringes parallel to the width of the precipitates suggesting the presence of interfacial dislocations which are expected to occur if the precipitates are semicoherent.

Dark-field microscopy of some precipitates indicated that these were segmented, with the segments arranged in a direction perpendicular to the length of the precipitate. This appearance was suggestive of internal twinning of the precipitate particles. However, conclusive diffraction evidence in this regard could not be obtained.

In dark-field imaging, it was also possible to see another type of precipitate, which appeared circular in cross section and was devoid of the fringe contrast observed in the rod-shaped precipitates. The SAD patterns indicated that these precipitates were of the Fe_2Mo phase.

d. *Specimens overaged at 640 °C*

The TEM investigations were carried out on samples subjected to overaging at 640 °C for 2 and 8 hours.

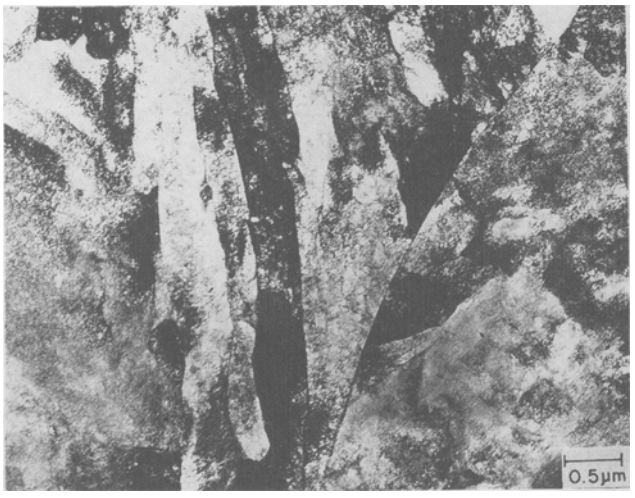

(*a*)

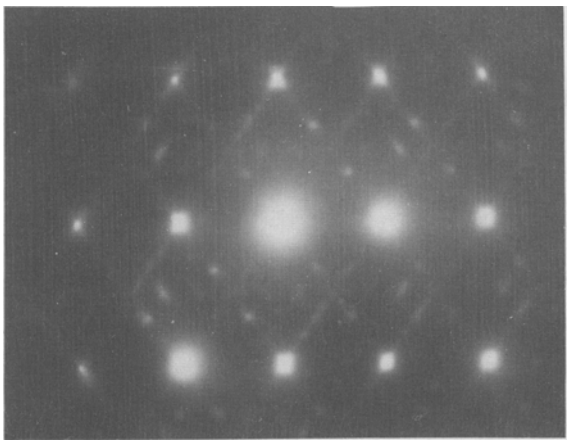

(*b*)

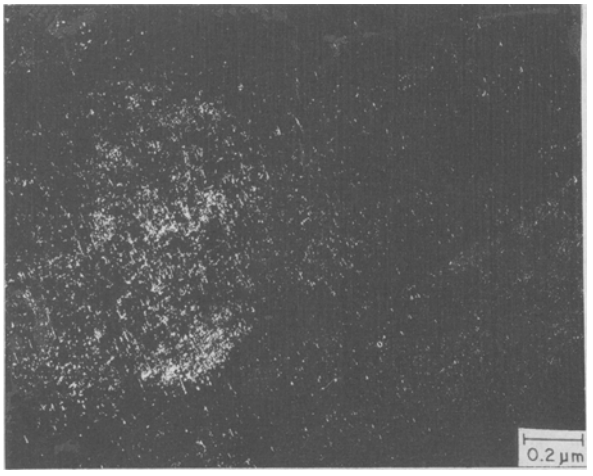

(*c*)

Fig. 5—(*a*) Microstructure of the material aged at 510 °C for 30 minutes. (*b*) $[011]_M$ SAD pattern showing precipitate spots and streaks besides the matrix reflections. (*c*) Dark-field micrograph using $(20\bar{2}0)$ Ni_3 (Ti, Mo) precipitate reflection.

In the specimen overaged for 2 hours, the basic microstructure comprised of parallel arrangement of laths of the martensite phase (Figure 9(a)). The dislocation arrangement within the lath was tangled, and the dislocation density was fairly large. The appearance of the laths was more or less similar to the martensitic structure observed in the as-solution treated sample, the main difference being the presence of a second phase at the lath boundaries as shown in Figure 9(b). The SAD pattern from these second phase regions showed that these were of the austenite phase. The orientation relationship between the austenite and the martensite phases was found to be of the Kurdjumov-Sachs (K-S) type:[11] $(110)_{bcc}$ // $(111)_{fcc}$ and $[111]_{bcc}$ // $[110]_{fcc}$.

In the specimens overaged for 8 hours at 640 °C, the matrix phase was found to be lath martensite. Within this martensite matrix, particles and pockets of other phases, including austenite, were found. This austenite phase had the following three morphologies.

(1) *Globular austenite*: This particular type of austenite (shown by the arrow in Figure 10(a)) had a globular morphology. The volume fraction of this type of austenite phase was quite small. It was found to obey the K-S orientation relationship with the martensite matrix (Figure 10(b)). Though a similar diffraction pattern has been obtained in earlier studies,[7] in this study, it was established that this pattern contained spots from the austenite phase also, and the dark-field microscopy using these spots indicated that these reflections belonged to the globular austenite phase which obeyed the K-S orientation relationship with the matrix.

(2) *Widmanstätten austenite*: This type of austenite morphology was found to be present mostly inside the martensite laths, as shown in Figure 10(c). These obeyed the K-S orientation relationship with the martensite phase.

(3) *Recrystallized austenite*: This morphology of the austenite, indicated by the arrow in Figure 10(d), formed mainly inside the martensite laths, had a platelike appearance. In some regions, this plate-shaped austenite appeared to have second phase particles embedded in it as shown by the arrow in Figure 10(e). The austenite plates were found to be twinned at some places

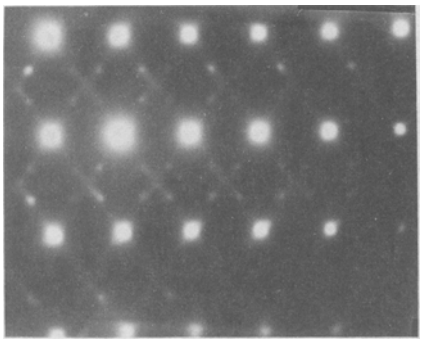

(*a*)

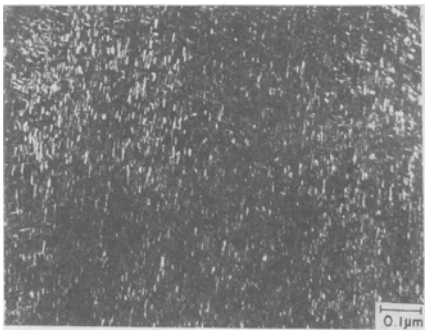

(*b*)

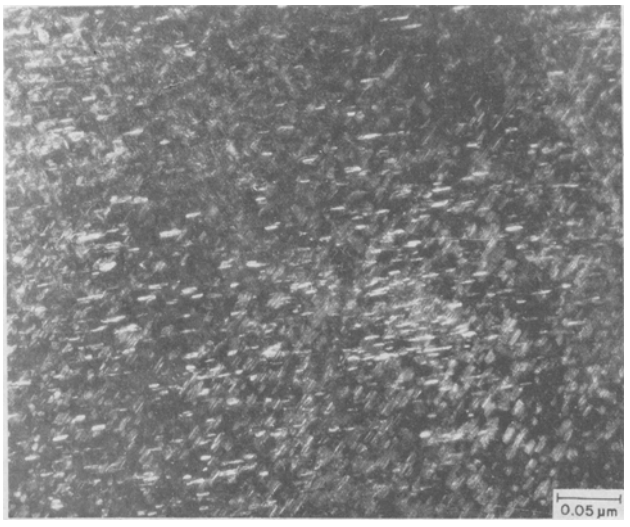

(*c*)

Fig. 6—(*a*) $[011]_M$ SAD pattern showing streaks and spots arising from precipitates. (*b*) Dark-field micrograph taken from the $(20\bar{2}2)$ Ni_3 (Ti, Mo) reflection showing precipitates of the Ni_3 (Ti, Mo) type. (*c*) Dark-field micrograph taken from the $(40\bar{4}2)$ Ni_3 (Ti, Mo) reflection showing fringe contrast from the precipitates.

(Figure 10(d)). These plates obeyed the K-S orientation relationship with the martensite phase.

Mostly one variant of the plate-shaped austenite phase was found to be present in a single lath of martensite. This fact becomes evident in the dark-field micrograph (Figure 10(e)). It was possible to see interfacial dislocations at the austenite-martensite interface.

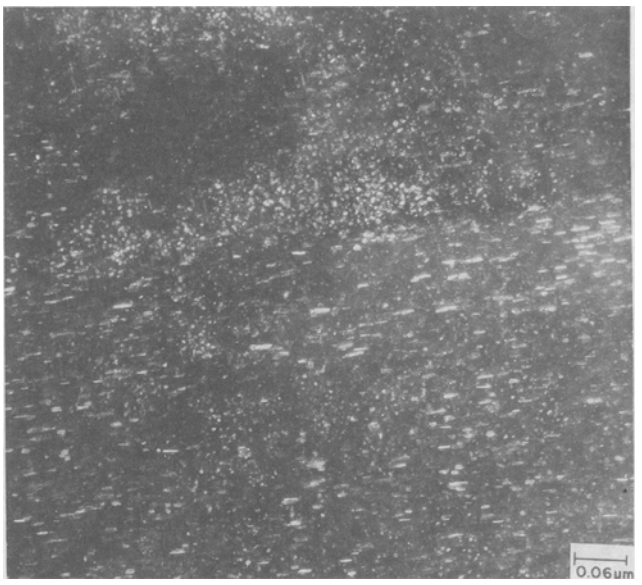

(*a*)

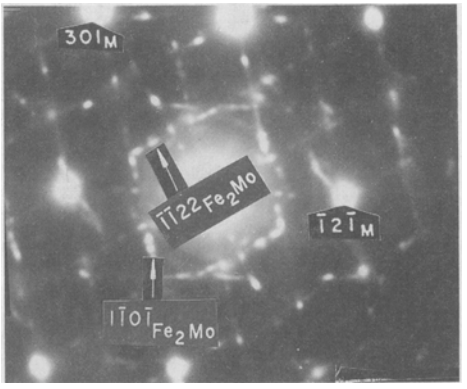

(*b*)

Fig. 7—(*a*) Dark-field micrograph taken from the $(\bar{1}\bar{1}22)$ Fe_2Mo reflection showing the spherical precipitate of the Fe_2Mo phase. (*b*) SAD pattern showing the Fe_2Mo reflections. Martensite zone axis [123] and Fe_2Mo zone axis $[\bar{5}\ 1\ 4\ 6]$.

Besides the austenite phase, the volume fraction of the Ni_3 (Ti, Mo) type intermetallic phase, which could be identified by electron diffraction, was also significant. The precipitates of the Ni_3 (Ti, Mo) type were found to have an average length of 130 nm and a width of about 16 nm. These showed a variety of fringe contrasts. Some of these were very similar to those arising from precipitates formed at lower temperatures and shorter aging time. Figure 11 shows precipitates having fringes parallel to their length and width.

Another striking feature of the SAD patterns obtained from the martensite matrix was the presence of weak diffraction spots at the $\{100\}_M$ locations (Figure 12). These can originate either due to B2 ordering or due to the $\{110\}_M$ reflections from the surface Fe_3O_4.[7] It has been established by Spooner *et al.*[12] that cobalt cannot induce long-range ordering. However, the existence of short-range ordering going beyond the first neighbor has been indicated by Rack *et al.*[13]

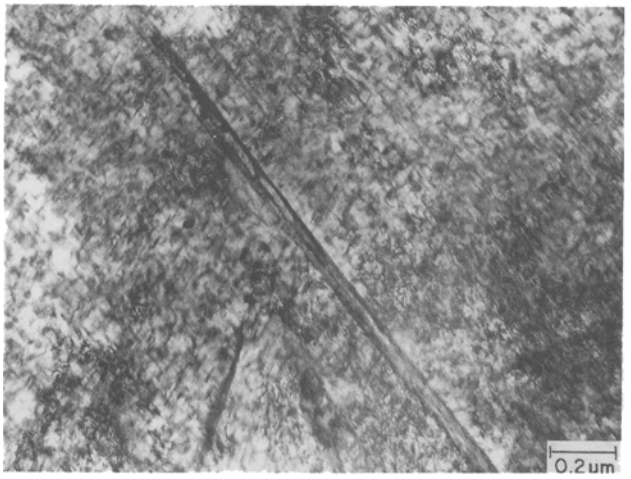

(a)

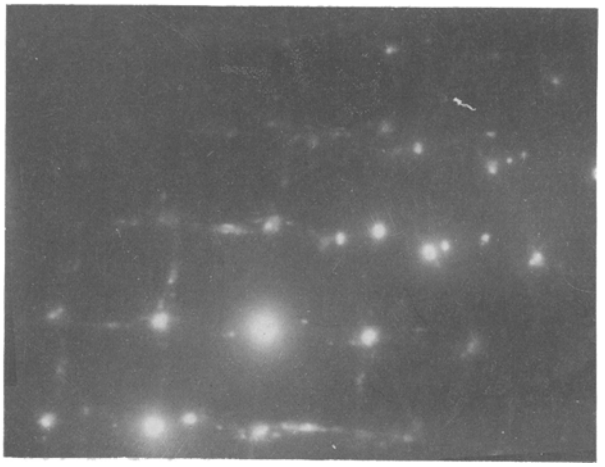

(b)

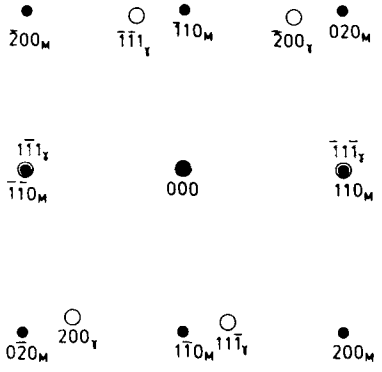

(c)

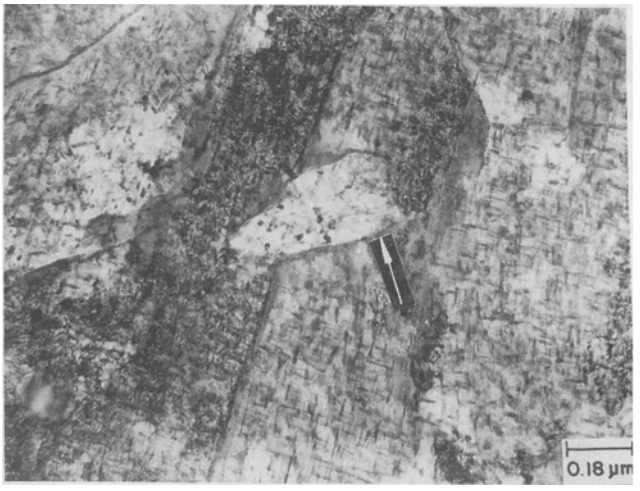

(d)

Fig. 8—(*a*) Bright-field micrograph showing interlath austenite. (*b*) SAD pattern from the region containing the interlath austenite, indicating N-W orientation relationship between the austenite and martensite phases. Austenite zone axis [011] and martensite zone axis [001]. (*c*) key to (b). (*d*) Recrystallized austenite (shown by the arrow) containing some spherical precipitates. (*e*) Presence of fringes parallel to Ni_3 (Ti, Mo) precipitate.

2. *Microstructure after deformation*

Microstructures of the alloy aged at 510 °C for 3 hours and at 575 °C for 8 hours were examined after deforming until fracture, in order to ascertain the nature of the dislocation precipitate interaction.

The microstructure of the alloy aged at 510 °C for 3 hours and deformed consisted of lath martensite (Figure 13(a)). Due to the high-dislocation density, it was not possible to image the dislocation structure very clearly. Extensive dark-field electron microscopy was carried out to examine the effect of deformation on the precipitates. A dark-field micrograph taken using $(20\bar{2}2)$ reflection of Ni_3 (Ti, Mo) showed that the dislocation-precipitate interaction was manifested as segmentation of the precipitates into small sections. The segments in several precipitates were found to be displaced with respect to each other (indicated by the arrows in Figure 13(b)).

The martensite lath morphology in a specimen aged at 575 °C for 8 hours and deformed is shown in Figure 14(a). The displacement of the segmented parts of the precipitates with respect to each other as observed in the case of the specimens aged at 510 °C for 3 hours could not be seen in this case (Figure 14(b)).

IV. DISCUSSION

A. *Maraging Reactions*

The effects of various alloying elements on the mechanical properties are fairly well documented in lower grades of maraging steels.[14–19] However, the maraging characteristics of the 350 grade steel has not yet been thoroughly examined. It was reported[13] that during the initial stages of aging, molybdenum atoms tend to cluster to form precipitates, and the cobalt atoms assume short-range ordered configurations. The rejection of nickel from

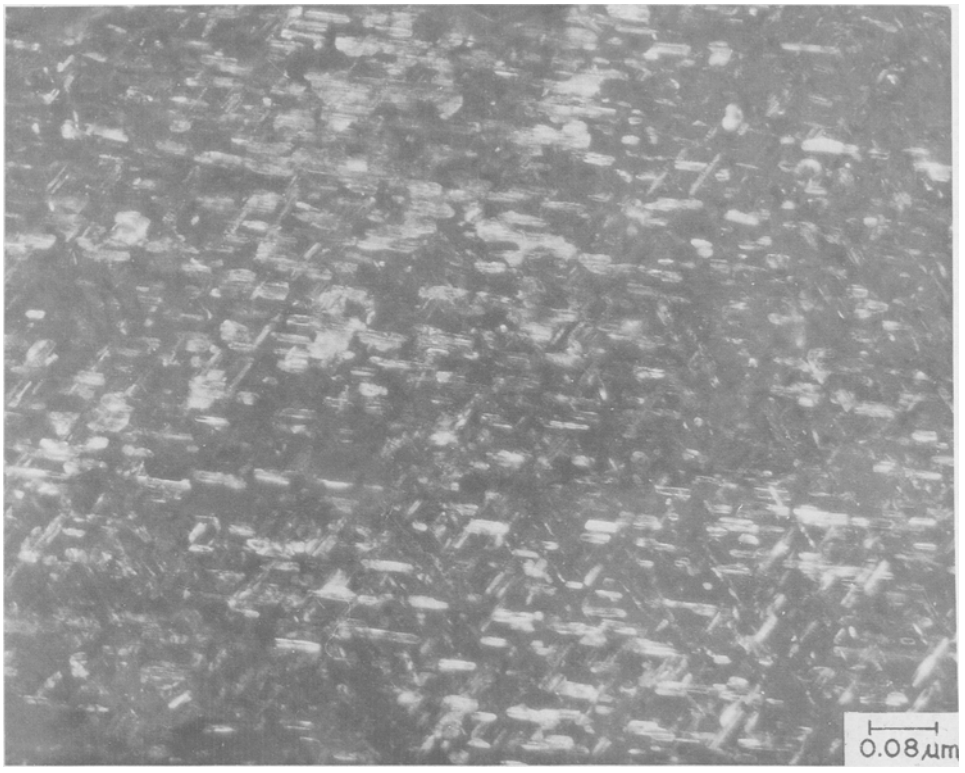

(*e*)

Fig. 8 Cont.—(*a*) Bright-field micrograph showing interlath austenite. (*b*) SAD pattern from the region containing the interlath austenite, indicating N-W orientation relationship between the austenite and martensite phases. Austenite zone axis [011] and martensite zone axis [001]. (*c*) key to (b). (*d*) Recrystallized austenite (shown by the arrow) containing some spherical precipitates. (*e*) Presence of fringes parallel to Ni_3 (Ti, Mo) precipitate.

the ordered Fe-Co regions and the clustering of molybdenum lead to the formation of Ni_3Mo precipitate. The regions lean in nickel serve as effective sites for the formation of FeTi. The presence of cobalt in a short-range order configuration principally alters the size and the extent of the subsequent Ni_3Mo precipitation by altering the local solubility of molybdenum. During the later stages of aging, the metastable precipitates coarsen. But at certain regions like prior austenite boundaries and martensite lath boundaries, dissolution of Ni_3Mo precipitates occurs, leading to local enrichment of nickel. These sites act as the nucleating centers for the formation of austenite. However, the addition of titanium in the high-strength grades (300 and 350) is reported to retard the austenite reversion. In the later stages of aging, titanium interacts with nickel to form Ni_3Ti,[20] leading to the depletion of nickel in the matrix, and prevents the nucleation of austenite. The results of the present investigation, however, did not agree with the reported observations. Samples aged to the peak-strength condition (510 °C for 3 hours) were found to contain precipitates of the Ni_3 (Ti, Mo) and Fe_2Mo types. Neither FeTi nor austenite could be detected in the peak-aged specimen. These aspects will be discussed in detail later in the context of the evolution of microstructure in the material during overaging.

B. *Maraging Kinetics*

An accurate estimation of the kinetics of precipitation in a maraging steel is difficult due to a variety of reasons. Since the material contains a large number of alloying elements, more than one type of precipitate is formed during aging. Moreover, due to the close similarities in structures and interplanar spacings of some of these intermetallics, identification often becomes difficult. Reversion of martensite to austenite, in addition to the intermetallic precipitates and the presence of coherency strains, make the precipitation process more complex. However, in the present case, the temperatures selected for evaluating the kinetics were such that the contribution from austenitic reversion was the least.

The hardness data were utilized in estimating the activation energy of the maraging reactions. The shape of the hardness curve showed the absence of any incubation period for the onset of precipitation, as reported by others.[21] By finding out the time taken to attain the peak hardness at each temperature and by fitting the data to an Arrhenius relation between time and temperature, an activation energy of 164 kJ/mol was obtained. This value of the activation energy is well below the typical values for the diffusion of titanium (272 kJ/mol) and for molybdenum (238 kJ/mol) in ferrite.[22] The lack of an incubation period for the onset of precipitation and the

low value of activation energy obtained could be justified in terms of the nucleation of precipitate on dislocations during the initial stages of aging, followed by accelerated growth by the pipe diffusion mechanism facilitated by a high-dislocation density.[19] The microstructure of the as-solution treated material was indeed found to have a high density of dislocations which persisted even after aging. It was alternatively suggested[21] that characteristics like the lack of an incubation period and a low-activation energy are due to the close fit between the precipitates and the matrix. Similar observations have been reported in a 17-4 PH stainless steel, where maraging caused the precipitation of elemental copper in a supersaturated martensitic matrix containing a high density of dislocations.[23] The similarity in the matrix structure in these two cases is consistent with the contention that the kinetics of precipitation in both the cases are controlled by the high-dislocation density in the matrix substructure.

C. *Microstructural Evolution during Aging and Overaging*

The martensite phase in this steel was of the massive type comprising colonies of elongated laths containing a high density of dislocations. It has been reported by Patterson and Wayman[24] that dislocations in structures of this kind tend to lie in {111} planes along ⟨111⟩ directions and are mostly of the screw type. In this study, the adjoining platelets were found to be twin related in several cases. The orientation relationships between the austenite and the martensite laths were found to be of the N-W and the K-S types.

In the early stages of aging of the martensite phase, streaks could be observed in diffraction patterns. It has been proposed by Vasudevan *et al.*[7] that streaking primarily originated due to the thinness of the precipitates and is enhanced if large strain fields are also associated with the precipitates. Based on the evidence obtained from SAD patterns, it was inferred by them that coherent zones, presumably enriched in titanium and molybdenum, form on dislocations in the early stages of precipitation. It is interesting to note that although profuse streaking could be observed in electron diffraction patterns of specimens aged at 510 °C and 575 °C this effect was absent in the specimen aged at 640 °C.

The identity of the precipitates forming during the initial stages of aging has not been unambiguously established. However, it has been generally agreed that the initial precipitates are of the Ni_3Mo or Ni_3Ti types.[1] The Ni_3Mo has an orthorhombic structure whereas the Ni_3Ti phase has a hexagonal structure.[7] It has recently been shown[7] that the nickel atoms in the Ni_3Ti unit cell can be replaced by iron or cobalt atoms and the titanium atoms by molybdenum. Therefore, a general formula of the type $(Ni, Fe, Co)_3 (Ti, Mo)$ has been assigned to these precipitates. The concentration of molybdenum and titanium in the precipitates is dictated by the relative amounts of these elements present in the alloy.

Two crystal structures have been reported in the case of the $(Ni, Fe, Co)_3 (Ti, Mo)$ phase: orthorhombic[25] and hexagonal.[7,3] However, it should be remembered in this context that the orthorhombic lattice can be viewed as a distorted hexagonal lattice. Most of the patterns obtained in this study could be explained in terms of the hexagonal structure.[7] The hexagonal $Ni_3 (Ti, Mo)$ phase is known to have the following orientational relationship with the body-centered cubic (bcc) matrix:

$$(0001)_\eta \,//\, (011)_M; \qquad [11\bar{2}0]_\eta \,//\, [1\bar{1}1]_M$$

Twelve different variants of this orientation relationship are possible. Vasudevan *et al.*[7] have used a computer simulation for generation of diffraction patterns of the Ni_3Ti phase. In this study, the construction of the diffraction patterns of different variants of the $Ni_3 (Ti, Mo)$ phase was carried out by a procedure similar to the one used by Sass *et al.*[26] for generation of diffraction patterns of the ω phase in a bcc matrix. The simulated diffraction patterns are shown in Figures 15(a) and (b). After taking the double diffraction effects into account, the simulated patterns were found to resemble the observed patterns (Figures 5(b), 6(a), and 10(b)) quite well. While comparing the generated and observed diffraction patterns, it should be noted that many of the precipitate reflections may be faint and often invisible in the observed

(*a*)

(*b*)

Fig. 9—(*a*) Parallel arrangement of laths of the martensite phase in specimens overaged at 640 °C for 2 hours. (*b*) Dark-field micrograph taken from the $(111)_A$ reflection showing an austenite phase at the lath boundaries.

(*a*)

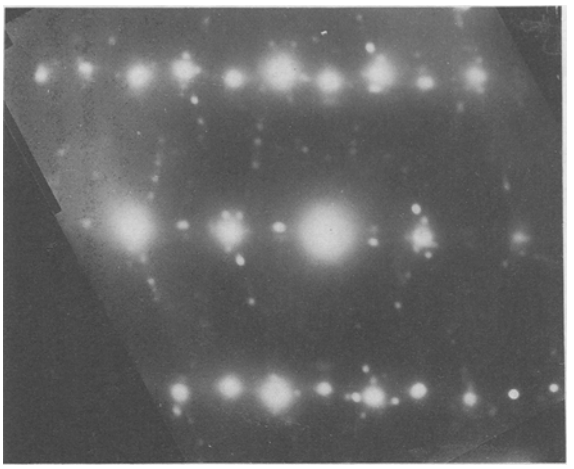

(*b*)

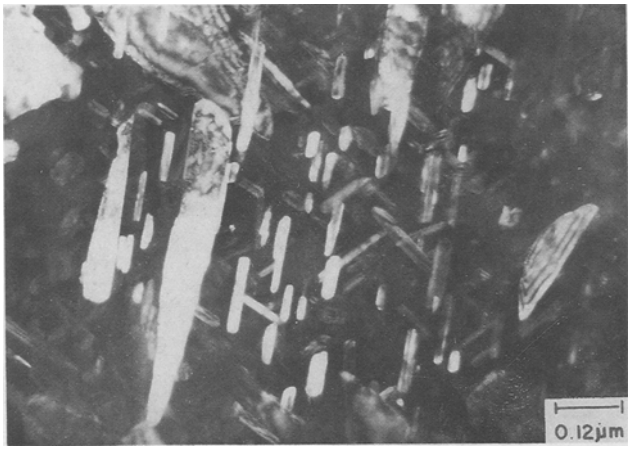

(*c*)

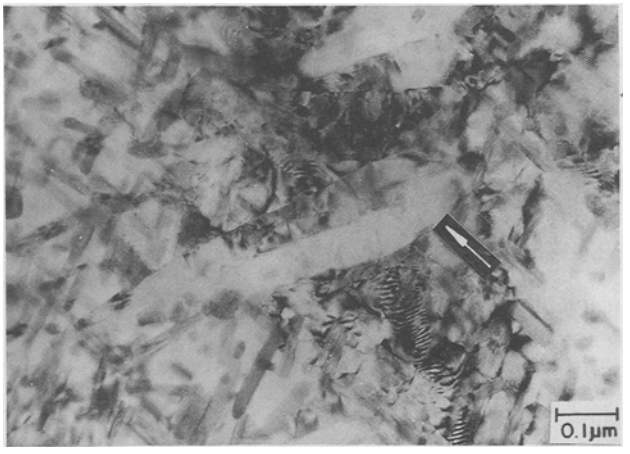

(*d*)

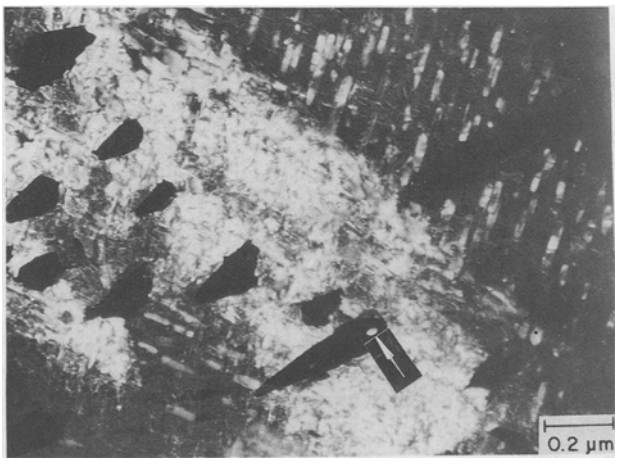

(*e*)

Fig. 10—(*a*) Dark-field micrograph using (220) reflection showing the globular austenite phase (shown by the arrow). (*b*) SAD pattern showing K-S orientation relationship between the globular austenite and the martensite. (*c*) Widmanstätten austenite phase inside the martensite lath. (*d*) Bright-field micrograph showing recrystallized austenite phase (shown by the arrow). (*e*) Dark-field micrograph showing the presence of second phase particles inside the austenite phase (indicated by the arrow).

Fig. 11—Bright-field micrograph showing fringes parallel to the length and the width of plates of the Ni_3 (Ti, Mo) type precipitate phase.

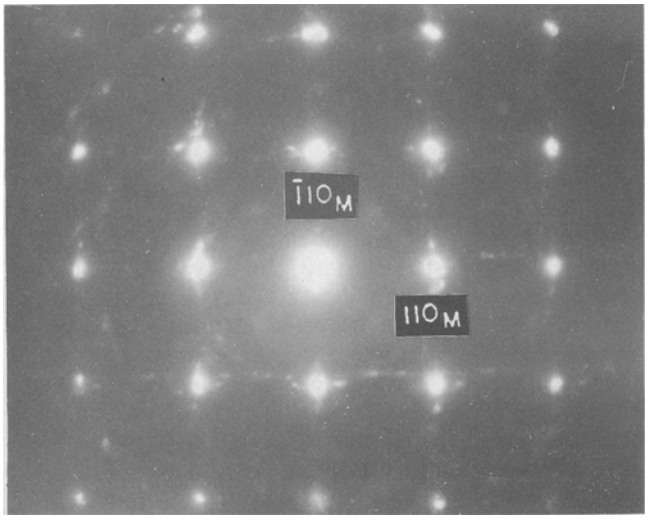

Fig. 12—$[001]_M$ SAD pattern showing weak diffraction spots arising possibly due to the presence of the Fe_3O_4 phase.

patterns.[7] In addition to the (Ni, Fe, Co)$_3$ (Ti, Mo) phase, the other phase of significance in the peak-aged condition is Fe_2Mo. This phase has a hexagonal structure with the following lattice parameters: $a_0 = 0.4745$ nm and $c_0 = 0.7754$ nm. It is isostructural with the $MgZn_2$ phase.[27] Two types of orientation relationships have been suggested between this phase and the bcc matrix in the Fe-Mo system.[28,29] Out of these, the following one was found to be more appropriate in the present context, (Figure 7(b))

$$(0001) \,//\, (011), \qquad [\bar{1}2\bar{1}0] \,//\, [0\bar{1}1]$$

As in the case of the Ni_3Ti lattice, substitution is possible in the Fe_2Mo lattice also. The iron atoms can be substituted by cobalt or nickel atoms and the molybdenum atoms can be replaced by titanium atoms. Hence, this phase should more appropriately be designated as the (Fe, Ni, Co)$_2$ (Ti, Mo) phase. This phase, which is believed to be responsible for the maintenance of high strength even on prolonged aging was found to have a spherical morphology. Though the formation of this phase could be seen at lower aging temperatures, it could not be observed at higher aging temperatures.

It has been suggested by Vasudevan *et al.*[7] that the lattice mismatch along the close-packed directions in the close-packed planes of the precipitate phase and the martensite matrix is about 2.22 pct. In order to accommodate this mismatch, a dislocation has to be present after about every 25 atomic planes at the precipitate-martensite interface, assuming the dislocation to be of the edge type, having a Burgers vector $\mathbf{b} = a/\langle 111 \rangle$. Precipitates smaller than 10 nm would, therefore, remain coherent; whereas, those larger than this would be semi-coherent. In this study, precipitates in the peak-aged specimen were about 40 nm in length on the average. In some of these larger precipitates, interfacial dislocations could be seen. However, in the smaller ones, the presence of interfacial dislocations could not be detected.

Micrographs obtained from specimens aged at 575 °C for 8 hours clearly indicated the presence of interfacial dislocations at the matrix-precipitate interface. These dislocations occurred in order to accommodate the precipitate-matrix misfit.

The observed contrast from the precipitate was found to change with the direction of the electron beam. The precipitates were found to exhibit two types of contrast: (1) Fringe contrast with the fringes lying parallel to the length of the precipitates. These fringes were symmetric in bright field and asymmetric in dark field and originated when the precipitate habit plane was inclined with respect to the electron beam; and (2) Dislocation contrast along the width of the precipitates, making the overall contrast quite complex. In some of the precipitates both types of contrast could be seen together.

D. *Morphology of Reverted Austenite*

Prolonged aging of the martensite leads to its reversion into the austenitic phase. The morphology of the reverted austenite is decided by the aging temperature and time. The first to form during aging is the matrix austenite. This is followed by the formation of lathlike austenite and finally the recrystallized austenite is formed.[30] The matrix austenite is known to form either along the prior austenite grain boundaries or it grows from the retained austenite.[30] The lathlike austenite, on the other hand, nucleates independently inside the martensite laths and also forms at the prior austenite grain boundaries. The packet-packet boundaries between the

(*a*)

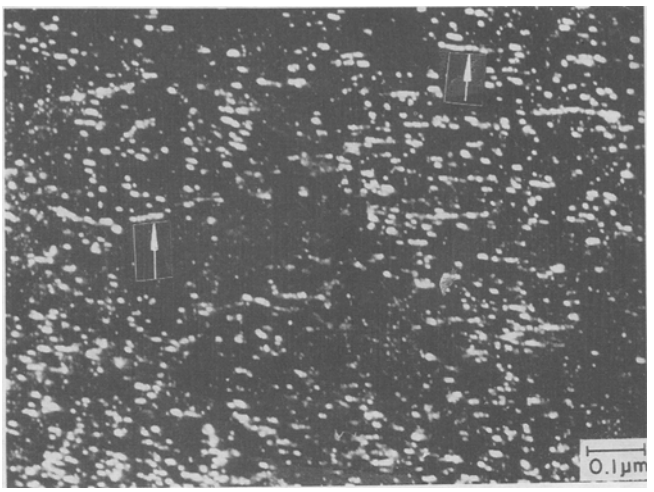

(*b*)

Fig. 13—(*a*) Martensite laths in peak-aged and deformed specimen showing high density of dislocations. (*b*) Dark-field micrograph obtained from $(20\bar{2}2)$ Ni_3 (Ti, Mo) reflection showing segmentation of precipitates (indicated by the arrow).

(*a*)

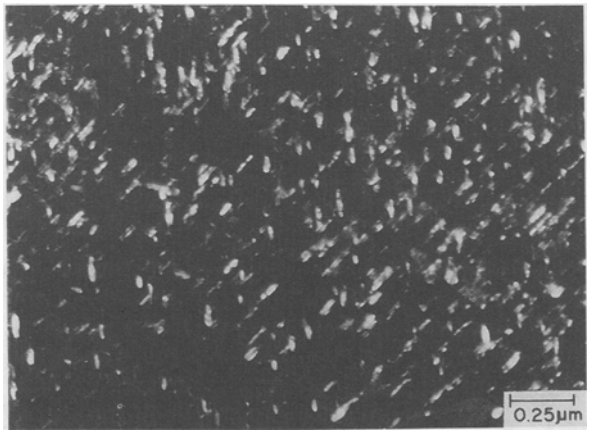

(*b*)

Fig. 14—(*a*) Martensite laths in an overaged and deformed specimen. (*b*) Dark-field micrograph obtained from the $(22\bar{4}0)$ Ni_3 (Ti, Mo) reflection.

martensite laths are the preferential sites for the nucleation of recrystallized austenite. In addition to the types of austenite mentioned previously, the formation of Widmanstätten austenite and globular austenite has also been reported.[30] The different types of austenite are reported to obey different types of orientation relationship with the martensite phase.[30]

In specimens overaged at 575 °C for 8 hours, the formation of lathlike and massive austenite could be noticed. The lathlike austenite was found to obey the N-W orientation relationship. In specimens aged at 640 °C for 8 hours, the formation of recrystallized austenite as well as Widmanstätten austenite could be seen. Austenite of these morphologies was found to obey the K-S orientation relationship with the martensite matrix. The recrystallized austenite and the Widmanstätten austenite were found to have undergone twinning. Presence of twins suggested that the formation of these types of austenite involved a shear motion. It has been shown by Shiang *et al.*[30] that twin related austenite plates can exist in cases of K-S, N-W, or intermediate orientation relationships between the martensite and austenite. The temperatures at which these two types of austenite were formed were very close to the A_s temperature of the alloy. Due to the segregation of the alloying elements to preferential sites during heating, the A_s temperature of the martensite at these locations could become equal to the aging temperature. As a result of this, the martensite could be expected to undergo a shear controlled austenitic transformation giving rise to the occurrence of twinning. The negligibly small strain energy associated with the nucleation of austenite[31] in the martensite could be expected to promote the formation of the former.

One of the most important differences between austenite formation at 640 °C and at lower temperatures like 575 °C is that in the latter case the intermetallic compounds form first, whereas in the former case the austenite forms first indicating rapid reversion.

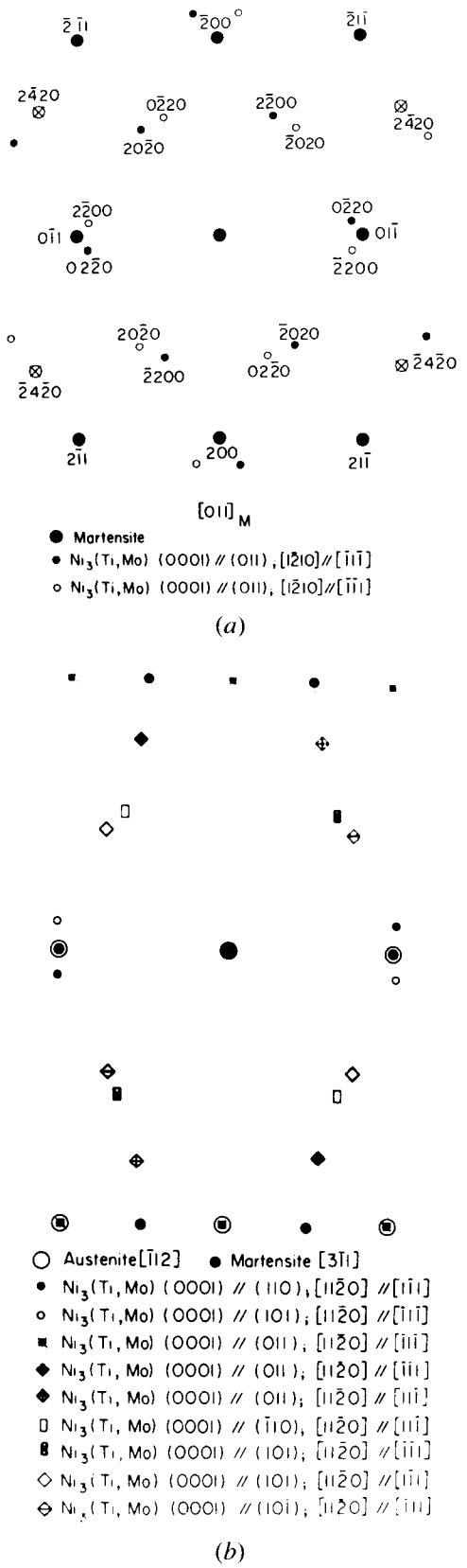

Fig. 15—Simulated SAD pattern showing the martensite reflections and different variants of the Ni_3 (Ti, Mo) phase. Zone axes are: (*a*) $[011]_M$ and (*b*) $[3\bar{1}1]_M$.

E. *Deformed Microstructure*

Due to the complex precipitation characteristics of 18Ni maraging steels, much work has not been carried out to probe the strengthening mechanisms operating in this alloy. Christian[32] has reported that in 18Ni maraging steels the Orowan model is capable of explaining the strength achieved during aging. However, apprehension regarding the strength of the precipitates to resist the shearing at the high-stress levels was expressed by him.

It is suggested that in the T-250 type of maraging steel, in the initial stages of aging, strengthening results due to the high stress required for dislocations to cut through Ni_3Ti precipitates.[7] The coarsening of the precipitates is likely to lead to change in the nature of the precipitates from coherent to semicoherent, and this brings about an increase in stress required to cut through the precipitates. At the peak-aged condition, the interparticle spacing is such that the dislocations are forced between them instead of cutting through them. Any further increase in particle size and spacing then leads to loss of strength.

In the present study, in the peak-aged condition, precipitate shearing could be clearly seen. The offset between the sheared parts of the precipitates was small because of the small total strain. These observations suggest that even in the peak-aged condition, order hardening and coherency strain hardening have very important contributions. The low work-hardening exponent of the peak-aged material also strongly suggests the occurrence of precipitate shearing as a principle mode of strengthening. Any theoretical estimation of the strengthening contribution of the precipitates in the material aged to peak strength necessitates the consideration of not only the Orowan equation, as has been done in several earlier studies,[7] but also the substantial contribution from order hardening and coherency strain hardening. Theoretical estimation of contributions from the latter two mechanisms requires knowledge of quantities like coherency strains, antiphase domain boundary energy, and so forth. Besides this, the manner in which these different contributions superimpose also remains to be ascertained. No attempt has been made in this study to make a theoretical estimation of the strengthening contribution of the precipitates.

The Orowan loops of the types seen in the case of superalloys[33] could not be seen in this alloy in the overaged condition. Though microstructural evidence could not be obtained to substantiate the occurrence of looping, the increase in the work-hardening exponent of overaged material can be considered as a consequence of the Orowan type of strengthening in the overaged condition.

V. CONCLUSIONS

From the observations made in this study, the following conclusions could be drawn.

1. The strengthening precipitates in this 350 grade maraging steel are the Ni_3 (Ti, Mo) and Fe_2Mo intermetallic phases.
2. The Ni_3 (Ti, Mo) type of phase forms by heterogeneous nucleation on the dislocations.
3. In the peak-aged condition, the deformation of the

material is associated with the shearing of precipitates by dislocations. The material in this condition exhibits an extremely low work hardening.
4. The martensite phase has a very strong tendency to revert to austenite on overaging. This and the coarsening of the strengthening precipitates lead to rapid loss of strength in the overaged specimens.
5. At temperatures where the reversion tendency is very high, the austenite formation precedes precipitation of intermetallic compounds.
6. Overaging causes an increase in the work hardening of the material, suggesting the occurrence of looping of precipitates by dislocations.

ACKNOWLEDGMENTS

The authors are thankful to Dr. C. Ganguly, Dr. S. Banerjee, and Dr. P. Mukhopadhyay for their keen interest in this work. The authors also are thankful to Dr. M. Sundararaman and Mr. E. Ramadasan for their valuable suggestions during the preparation of the manuscript.

REFERENCES

1. S. Floreen: *Met. Rev.*, 1968, vol. 13, pp. 115-28.
2. G.W. Tuffnell and R.N. Cairns: *Trans. ASM*, 1968, vol. 61, pp. 798-806.
3. J.B. Lecompte, C. Servant, and G. Cizon: *J. Mater. Sci.*, 1985, vol. 20, pp. 3339-52.
4. J. Singh and C.M. Wayman: *Mater. Sci. Eng.*, 1987, vol. 94, pp. 233-42.
5. L.T. Shiang and C.M. Wayman: *Metallography*, 1988, vol. 21, pp. 399-423.
6. D.M. Vanderwalker: *Metall. Trans. A*, 1987, vol. 18A, pp. 1191-94.
7. V.K. Vasudevan, S.J. Kim, and C.M. Wayman: *Metall. Trans. A*, vol. 21A, 1990, pp. 2655-68.
8. P. Ludwick: *Elemente Der Technologischen Mechanik*, Springer-Verlag, Berlin, 1909, p. 32.
9. Z. Nishiyama: *Sci. Rep. Tokohu Univ.*, 1934, vol. 23, p. 638.
10. G. Wassermann: *Arch. Eisenhütt*, 1993, vol. 16, p. 647.
11. G. Kudjumov and G. Sachs: *Z. Phys.*, 1930, vol. 64, p. 325.
12. S. Spooner, H.J. Rack, and D. Kalish: *Metall.*, 1971, vol. 2, pp. 2306-08.
13. H.J. Rack and D. Kalish: *Metall. Trans.*, 1971, vol. 2, pp. 3011-20.
14. R.B. Banerjee and J.J. Hauser: *Technical Report No. AFML-TR-66-166*, Air Force Materials Lab., Wright-Patterson AFB, Ohio (USA), 1966.
15. R.F. Decker, J.T. Eash, and A.J. Goldman: *Trans. Q. ASM*, 1962, vol. 55, pp. 58-76.
16. C.J. Novak and L.M. Diran: *J. Met.*, 1963, vol. 15, pp. 200-04.
17. S. Floreen and G.R. Speich: *Trans. Q. ASM*, 1964, vol. 57, pp. 714-26.
18. R.F. Decker: Proc. Symp. *Relation between the Structure and Properties of Metals*, NPL, Teddington, England, 1963, pp. 648-71.
19. M.D. Perkas: *Met. Sci. Heat Treat.*, 1968, vol. 6, pp. 415-25.
20. D.T. Peters: *Trans. Q. ASM*, 1968, vol. 61, pp. 62-67.
21. D.T. Peters and S. Floreen: *Trans. AIME*, 1969, vol. 245, pp. 2021-26.
22. M.K. Krishtal: in *Diffusion Processes in Iron Alloys*, Translated from Russian by the Israel Programme for Scientific Translations Ltd., Jerusalem, Israel, 1970, pp. 175-203.
23. U.K. Viswanathan, P.K.K. Nayar, and R. Krishnan: *Mater. Sci. Technol.*, 1989, vol. 5, pp. 346-49.
24. R.L. Patterson and C.M. Wayman: *Acta Metall.*, 1966, vol. 14, pp. 347-69.
25. W.A. Spitzig, J.M. Chilton, and C.J. Barton: *Trans. ASM*, 1968, vol. 61, pp. 299-303.
26. S.L. Sass: *Trans. AIME*, 1969, vol. 245, pp. 1836-38.
27. P. Villars and L.D. Calvert: *Pearson's Handbook of Crystallographic Data for Intermetallic Phases*, ASM, Metals Park, OH, 1985, vol. 3, p. 2905.
28. J. Higgins and P. Wilkes: *Phil. Mag.*, 1972, vol. 25, pp. 599-623.
29. J.P. Michel: *Mem. Sci. Rev. Met.*, 1971, vol. 58, pp. 785-92.
30. L.T. Shiang and C.M. Wayman: *Metallography*, 1988, vol. 21, pp. 425-50.
31. S. Floreen: *Trans. Q. ASM*, 1964, vol. 57, pp. 38-47.
32. J.W. Christian: *Strengthening Methods in Crystals*, A. Kelly and R. Nicholson, eds., Elsevier Publishing Co., Amsterdam, 1971, pp. 261-325.
33. B. Lerch and V. Gerold: *Acta Metall.*, 1985, vol. 33, pp. 1709-16.